Electrochemical Behaviour of Nb-Doped Anatase TiO2 Microbeads in an Ionic Liquid Electrolyte

doi.org/10.1002/batt.202000076

Electrochemical Behaviour of Nb-Doped Anatase TiO_2 Microbeads in an Ionic Liquid Electrolyte

Simon Lindberg,[a] Carmen Cavallo,[a, b] Giulio Calcagno,[c] Adriana M. Navarro-Suárez,[a] Patrik Johansson,[a] and Aleksandar Matic*[a]

TiO_2 is a promising material for high-power battery and supercapacitor applications. However, in general TiO_2 suffers from an initial irreversible capacity that limits its use in different applications. A combination of a microbead morphology, Nb-doping, and the use of an ionic liquid electrolyte is shown to significantly decrease the irreversible capacity loss. A change in the electrochemical response in the first cycles indicates formation of a solid–electrolyte interphase (SEI) or a modification of the structure of the surface layer of the TiO_2/Nb microbeads, which apparently stabilises the performance. The change in the response is manifested in an increased charge transfer resistance and the presence of two charge transfer contributions. During prolonged cycling the TiO_2/Nb electrode shows an excellent stability over 5000 cycles. Ex situ analysis after cycling shows that the overall microbead morphology is intact and that there are no changes in the crystal structure. However, a decrease in the intensity of the XRD pattern can point to a decrease in size of the nanocrystals building up the microbeads or the formation of amorphous phases.

1. Introduction

Supercapacitors can play an important role in future energy systems in parallel with Li-ion batteries.[1] Compared to batteries, supercapacitors possess higher power density, longer cycle lifetime, lower cost of active materials and increased safety.[2] However, supercapacitors are hampered by comparatively low energy densities. For many applications, such as electromobility, an increase in energy density from 2–8 Wh kg^{-1} to $>$15 Wh kg^{-1} on a cell level is desired.[1] A common strategy to improve the energy density of supercapacitors is to replace the active material, typically carbon, in one of the electrodes with a battery-type active material that can store energy through electrochemical reactions, together forming a hybrid supercapacitor. In order to maintain the advantage of supercapacitors, high-power performance of the battery-type active material is essential.

TiO_2 has been studied extensively for its high-power performance in batteries[3,4] as well as in hybrid supercapacitors.[5] The Li-insertion/extraction in TiO_2 has been described previously for conventional organic electrolytes and found to depend on the structure of the TiO_2 material.[6] In anatase TiO_2 Li-insertion occurs in different stages, a pseudocapacitive behaviour with interfacial energy storage up to −1.4 V (vs Ag/Ag$^+$) (corresponding to 1.75 V (vs Li/Li$^+$), two phase bulk intercalation around −1.4 V (vs Ag/Ag$^+$) and a solid solution of Li and TiO_2 at higher potentials.[7] Overall the Li-insertion and extraction mechanism can be described by [Eq. (1)]:

$$\mathrm{Ti(IV)O_2} + x\mathrm{Li^+} + x\mathrm{e^-} \leftrightarrow \mathrm{Li}_x\mathrm{Ti(III)O_2}\ (x \leq 1) \quad (1)$$

For fast and reversible reaction, the Li-insertion is usually confined to $x \leq 0.5$, in which case the theoretical capacity is limited to 168 mAh g^{-1}.[8]

Different strategies have been proposed to improve the high-power performance, including new polymorphs,[9–12] creating oxygen deficiencies[10,13] or doping with hetero-atoms,[14,15] with the aim to optimize structure, morphology and to increase the electronic conductivity to ensure fast kinetics of the electrochemical reactions. However, an irreversible capacity loss when using common organic electrolytes limits the applicability of TiO_2.[16,17] To mitigate this problem different electrolyte formulations have been proposed and a promising route is the use of ionic liquid (IL) based electrolytes.[18,19] It has been suggested that the presence of an IL stabilizes the surface of the active material and in this way reduces the irreversible capacity loss. ILs can in addition also improve the safety and the electrochemical stability.[20,21] ILs have so far typically been used mixed with organic solvents and studies of the electrochemical behaviour of TiO_2 with neat IL electrolytes are scarce.[22]

[a] S. Lindberg, Dr. C. Cavallo, Dr. A. M. Navarro-Suárez, Prof. P. Johansson, Prof. A. Matic
Department of Physics, Chalmers University of Technology
Material Physics
41296 Gothenburg, Sweden
E-mail: matic@chalmers.se
[b] Dr. C. Cavallo
Department of Chemistry, Oslo University
Center for Materials Science and Nanotechnology
0371 Oslo, Norway
[c] G. Calcagno
Department of Chemistry and Chemical engineering
Chalmers University of Technology, Applied Chemistry
41296 Gothenburg, Sweden

Supporting information for this article is available on the WWW under https://doi.org/10.1002/batt.202000076

We have recently reported on a new route to achieve high power-performance and good cycling stability by a microbead morphology of anatase TiO_2.[23] Another route that can be explored is doping by aliovalent ions to tune the electronic properties of anatase and a few studies have been reported on doping TiO_2 (rutile and/or anatase) with Nb^{5+}.[24,25] It was found that Nb doping can increase the rate capability by improved Li^+ diffusion and electronic conductivity.[24,25] Here we combine these two routes by investigating a new TiO_2/Nb microbead material in a hybrid supercapacitor set-up using an IL-based electrolyte. In particular we target the electrochemical response of the material, the effect on irreversible capacity loss, and the role of Nb-doping in stabilizing and improving the cycling performance.

2. Results and Discussion

The morphology of the pristine TiO_2/Nb micro-bead material with 1% Nb content is shown in Figure 1. The diameter of the beads is about 1 µm and it has previously been shown that they are built up of anatase nano-crystallites (around 25 nm).[23] The crystal structure and morphology are both independent of the Nb doping concentration.[23,26]

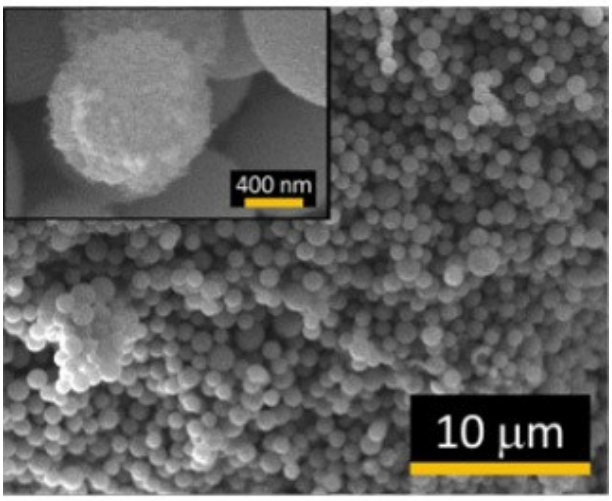

Figure 1. SEM image of the anatase TiO_2/Nb microbeads with 1% Nb content.

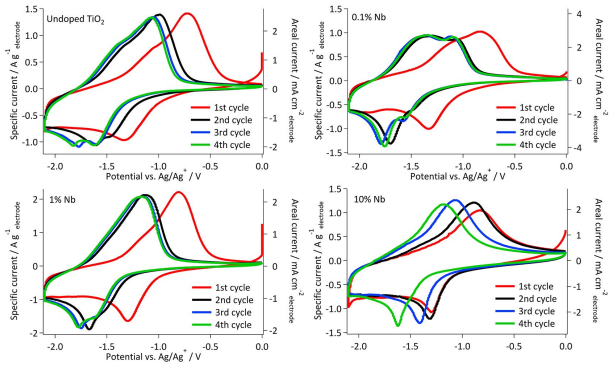

Figure 2. CVs of the first four cycles of cells with the undoped TiO_2 material and the three different Nb-doping concentrations acquired at 10 $mV s^{-1}$.

To investigate the electrochemical response and understand the charge transfer processes of the TiO_2/Nb material in the IL-based electrolyte we applied CV, EIS and CC cycling. The four first CVs for the different Nb-doping concentrations, and for the undoped reference material, are shown in Figure 2. The CV response in the 1st cycle is similar for the all electrodes and are similar to previous results for anatase.[16,18] The insertion peak in the first cycle is located around −1.3 to −1.4 V (vs Ag/Ag^+) and can thus be related to the two-phase intercalation region.[19] Furthermore, in the first cycle there is a continuous narrowing of the insertion peak with Nb-doping, which indicates an improved electron transfer in the electrode during Li insertion. There is also a systematic decrease in the peak separation, between insertion and extraction, with increased Nb-doping. The biggest change is observed going from the undoped material to 0.1% doping and with further addition of Nb-ions the decrease continues, but to less extent. The decreased peak separation indicates more reversible electrochemical processes and might be attributed to higher Li^+ concentration accumulated at the surface. The results indicate that a small amount of Nb has the ability to stabilize the structure which could be related to reduced strain during lithium insertion, as will be discussed further below.

In the CVs from the 2nd cycle there is a clear shift of both the insertion and extraction peaks to lower potentials for the electrodes with the undoped, 0.1% Nb and 1% Nb materials. Thus, the contribution from charge storage at the surface now dominates and the bulk contribution is decreased. In addition, the insertion peak is split into two distinct components. After the 2nd cycle no major changes occur in the CVs for these three materials. Overall, the shape of the CVs in the 2nd cycle have a resemblance to the CVs previously reported for the TiO_2(B) polymorph,[27–29] and could indicate that some kind of structural change has occurred at the surface of the microbeads. With 10% Nb doping, the CV evolves a bit differently with cycling. The shift of the peaks is more gradual from the 2nd to the 4th cycle and only one extraction and one insertion peak is observed.

The discharge capacities over the first four cycles were calculated by integrating the CVs. From this analysis discharge capacities in the range 19–32 $mAh g^{-1}$ are found. Thus, only 10–20% of the theoretical capacity of the material is utilized which underlines that only a surface layer of the TiO_2/Nb microbeads is lithiated. The initial capacity loss is limited and found to be 12% for the electrode with undoped TiO_2 and decreases further with Nb-doping, 10% and 7% for 0.1% and 1% Nb-doping, respectively. For the electrode with 10% Nb the capacity actually increases with 3%. The initial capacity losses are substantially smaller than values reported literature which around 40%.[30,31] The origin of the irreversible capacity loss has been explained by strain in the structure induced by Li-insertion[32] or different parasitic reactions at the surface, restricting lithium diffusion.[33] The rather low irreversible capacity losses for our materials indicate that the microbeads

are more stable and might develop some surface modifications with the IL-based electrolyte which improves the stability and doping with Nb seems to further stabilize the material.

EIS analysis was used to investigate any possible changes in the electron transfer processes. Starting with the reference LP30 electrolyte, which is known to be stable to low potentials and to not form a traditional solid electrolyte interphase (SEI) on TiO_2,[34] only a slight evolution of the frequency response after the initial cycle is found, see Figure 3a. In contrast, the IL-based electrolyte shows an increase of the semi-circle radius after four cycles, Figure 3b, reflecting an increase in the charge transfer resistance as commonly found when an SEI is formed or from other surface modifications. Similar changes in the EIS spectra upon cycling have been reported previously for IL-based electrolytes with carbon based electrodes and related to SEI formation.[35,36] Furthermore, with increased Nb-content there is a decrease in the semi-circle radius reflecting reduction in the charge transfer resistance in the electrode, Figure 3c. Thus, there is a clear influence of Nb on the charge transfer process which could be related to the difference cohesive energies between the two phases $LiTi_2O_4$ and $LiNb_2O_4$[37,38] and thus also thermodynamically infers that the Nb-doped structure is less stable and more easily subject to accepting (electronic) structure changes such as Li^+ intercalation.

The formation of an SEI, or other non-reversible reactions, should also be manifested in a reduced coulombic efficiency (CE).[39] The CEs calculated from the CVs, Figure 4, show that some side reactions occur in the first two cycles, but that there is a stabilization with further cycling. The exception is the 10% Nb material which shows a slower increase of the CE and a stabilization only after the 3rd cycle.

To investigate how the charge transfer resistance changes during the initial cycles, EIS was performed at different potentials: 0, −0.9 and −2.1 V vs. Ag/Ag^+ during charge and discharge of the undoped TiO_2 electrode, see Figure 5. When the potential is lowered, and lithium is inserted, the charge transfer resistance is reduced, illustrated by a decreased size of the semi-circle, which is in agreement with previous results for other Li-insertion materials.[40] When the electrode is delithiated to 0 V at the end of the 1st cycle the charge transfer resistance has increased compared to before cycling. In the 2nd cycle the charge transfer resistance is still reduced upon Li-insertion, but the effect is smaller. At −0.9 V it is almost the same as at 0 V, which can be explained by the peak shift of the insertion peak, i.e., at −0.9 V in the 2nd cycle no, or very few, Li-ions have been inserted, thus the charge transfer resistance is unchanged. In the 2nd cycle a second semi-circle, visible to the left of the large semi-circle is also present in the spectra. It indicates that there

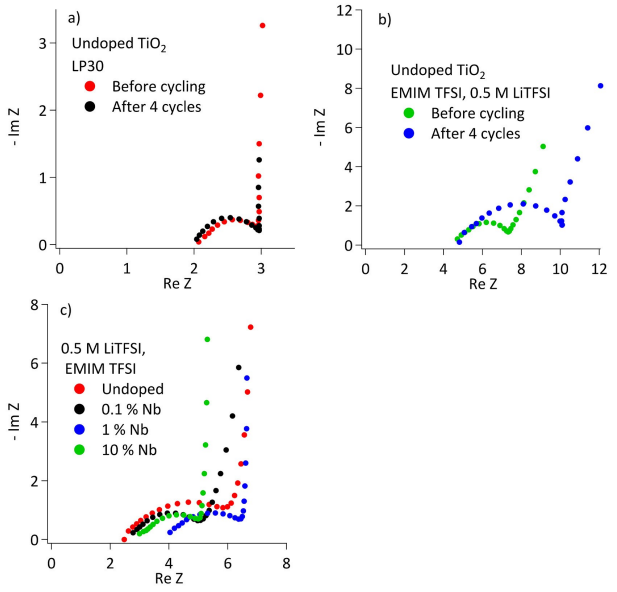

Figure 3. EIS-spectra of: TiO_2/Nb electrodes in a) 0.5 M LiTFSI in EMIMTFSI at OCV, b) before cycling and after four cycles of undoped TiO_2 in LP30, and c) 0.5 M LiTFSI in EMIMTFSI.

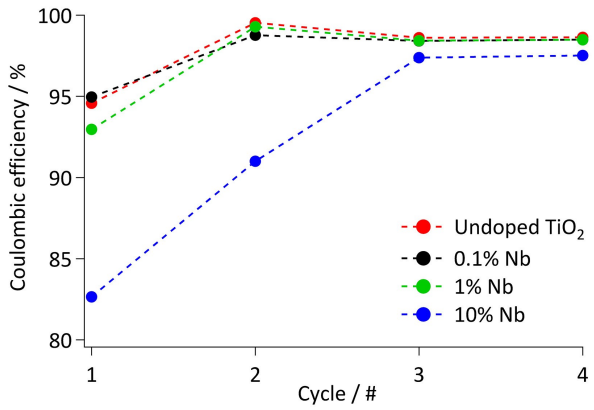

Figure 4. Comparison of coulombic efficiencies, calculated from the CVs in Figure 2, as a function of cycle number for different Nb concentrations.

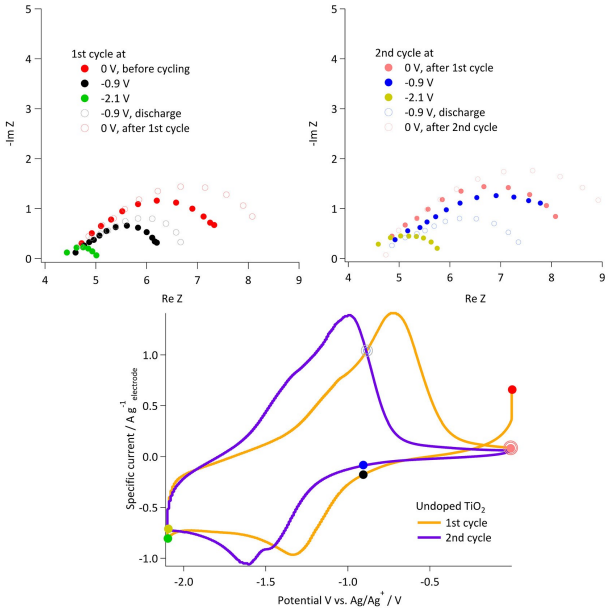

Figure 5. EIS of the undoped TiO_2 electrode at different potentials in the 1st (left) and 2nd (right) cycles with 0.5 M LiTFSI in EMIMTFSI. Investigated potentials are indicated in the CVs from the first and second cycles (bottom).

is a second phase forming in the material with a separate charge transfer resistance in agreement with the formation of co-existing TiO_2-phases at the surface as discussed above and in the literature.[41]

To evaluate the capacity performance of the electrodes CC cycling was performed and the results are shown in Figure 6. For undoped TiO_2 and the electrodes with 0.1% and 1% Nb doping the potential profiles are similar, showing pronounced plateaus, indicating that the insertion/extraction mechanism is similar. The electrode with 10% Nb doping displays a somewhat different voltage profile, with less marked plateaus and at the higher current densities the profile shows a high degree of linearity. Linear potential profiles for insertion type materials can be ascribed to an increased contribution of surface storage sites for lithium,[42] and that at high Nb content Li-ion interaction is restricted to the surface. Increasing the current density, the profiles become more linear in all samples, which is expected since the charge storage will be more and more confined to the surface and a larger contribution to the capacity comes from a double layer charge storage mechanism.

The capacity at the different current densities is calculated from the CC cycling, Figure 7. When the current density is increased the capacity decreases, as expected. However, upon increased Nb-concentration there is a dramatic improvement in the capacity retention as a function of cycling rate. The highest capacity is obtained for 1% Nb doping for all current densities and it also shows the best capacity retention, 75% of the initial capacity is retained at 20 $A g^{-1}$ compared to 30% for the undoped material. In a prolonged cycling test at 10 $A g^{-1}$ this electrode reveals a stable capacity over 5000 cycles and the CE is around 96% throughout cycling – in agreement with previous results using IL-based electrolytes and explained by the relatively low conductivity of the electrolyte.[19]

The stable behaviour under prolonged cycling points to stability of the structure and morphology of the material. To investigate if any changes of the electrode morphology, such as cracked particles, have occurred, SEM-images before and after prolonged cycling were compared and no changes can be observed, see Figure 8a–b. The TiO_2 particles remain intact and well dispersed in the carbon matrix, the only feature that separates the two images are residuals from the glass fibre separator found in the image of the electrode after cycling.

The effect of cycling on the crystal structure of the TiO_2/Nb particles is investigated by XRD before and after 5000 cycles, see Figure 8c–e. The diffractograms show no signatures of new structures formed during cycling, but if changes are limited to the surface, the contributions to the diffraction patterns might be too small to be discerned. Though, a reduction in the intensity of the diffraction peaks after cycling, which could be related to reduced crystallite size or formation of amorphous phases, is observed. There is also a slight shift in the peak positions. This shift is largest in the diffraction patterns from the undoped sample and can be related to strain introduced with Li-insertion and indicates that the presence of Nb-ions stabilizes the structure. Rietveld Refinement on the data provides a quantitative analysis of the XRD patterns and the parameters obtained in the analysis are reported in Table S1. Both the cell parameters and the particle size increases slightly

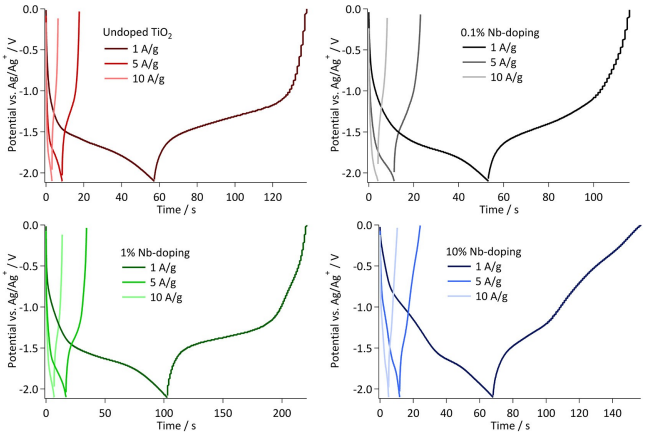

Figure 6. Potential profiles at current densities 1, 5 and 10 $A g^{-1}$ of the different electrodes with 0.5 M LiTFSI in EMIMTFSI.

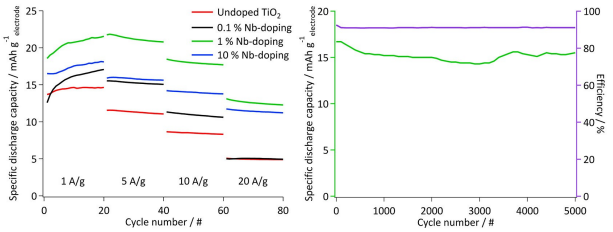

Figure 7. Specific capacities at different current densities (left) and cycle lifetime of the electrode with 1% Nb-doping at 10 $A g^{-1}$ (right).

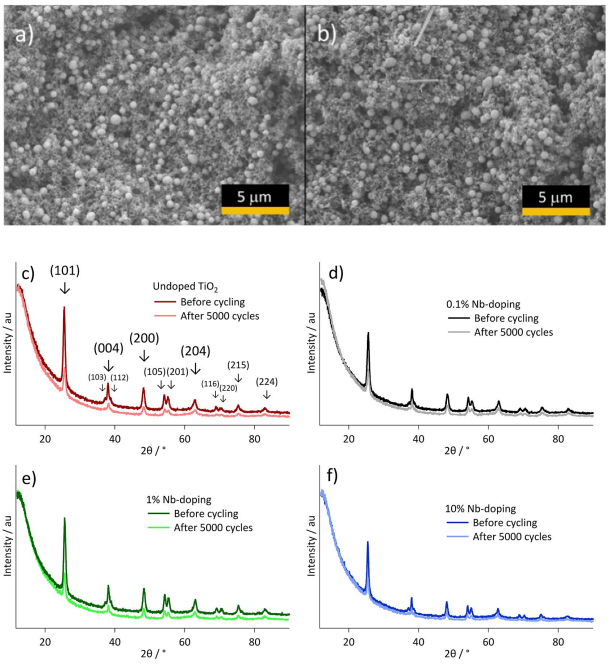

Figure 8. Comparison of SEM-images of the TiO_2 electrode with 1% Nb doping a) before, b) after 5000 cycles and c-d) the XRD patterns for the four different electrodes acquired before and after 5000 cycles.

with niobium doping, the former due to the difference in ionic radius of Ti^{4+} (0.64 Å) and Nb^{5+} (0.605 Å) and the formation of a substitutional solid solution.[24,26] After cycling, there is virtually no change in the particle size (within error bars), but a slight increase of lattice parameters can be observed.

To further investigate potential surface modifications as a result of cycling XPS measurements were performed on electrodes with 1% Nb doping in the pristine state, after the initial 10 CV cycles and after 5000 cycles. The results in Figures 9 and S2 show a change in the XPS spectra as a function of cycling. In the pristine material we find as expected contributions from Ti, Nb, O and C. The origin of the carbon peak in the pristine material is related to the added conducting carbon and the PVDF binder. As the electrode is cycled the surface composition changes and spectral components corresponding to surface groups containing oxygen, sulfur and nitrogen appear. The presence of nitrogen is explained by the decomposition of both EMIM cations and TFSI anions, previously described[43,44] and sulfur originates only from the decomposition of the TFSI anion. These contributions are present from the initial cycles and shows that and interphase layer is formed directly upon cycling and that it is stable over extended cycling. The decrease in the intensity of the Ti2p peaks further strengthens the hypothesis that an interphase layer is formed of decomposed electrolyte and covers the active material. The Ti2p of the pristine electrode is assigned to Ti^{4+} species, however, the bonding energy is slightly higher than previously reported,[45] which is explained by the charge compensation of the added Nb-atoms.[46] After the initial cycling a shift in the peaks towards lower energies is observed potentially pointing to a decrease of Nb concentration in the surface layer.

3. Conclusions

We have investigated the electrochemical response of a Nb-doped TiO_2 electrode material in an IL-based electrolyte. We show that with the combination of Nb-doping and microbead morphology anatase TiO_2 can show excellent cycling stability in an IL-based electrolyte without a large irreversible capacity loss.

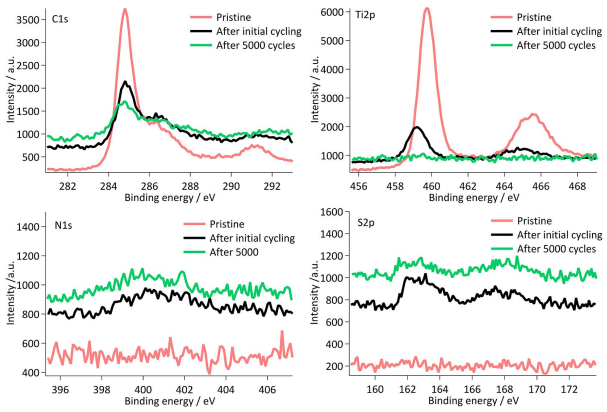

Figure 9. The XPS spectra of the C1s, Ti2p, N1s and S2p peaks of electrodes with 1% Nb-doping.

In the first cycles there is a modification of the surface of the active material, potentially with the formation of an SEI with the IL-based electrolyte. There is also a change from bulk charge storage to surface charge storage in the first cycles. The introduction of Nb-doping is shown to lower the charge transfer resistance of the electrode which is further supported by narrowing of the peaks and reduced the peak separation in the CVs from the first cycles. Through a prolonged cycling test (5000 cycles) we also demonstrate that the microbead morphology and crystal structure remain intact and that the presence of Nb-doping stabilizes the structure.

Experimental Section

Mesoporous anatase TiO_2 beads doped with 0.1 at%, 1.0 at% and 10 at% of Nb were synthesized following a previously reported solvothermal method.[26,47] Hydrolysis of titanium isopropoxide (TIP) in hydroalcoholic medium for 18 h with hexadecylamine (HDA) and Potassium Chloride (KCl) is controlled to allow the formation of the bead structure. HDA is necessary as a structure-directing agent and KCl to regulate the ionic strength. The hydrolysis is followed by autoclaving at 160 °C in hydroalcoholic ammonia for 16 h and calcination at 500 °C for 2 h in air. Niobium was introduced by substituting the appropriate amount of TIP with niobium (V) ethoxide during the synthesis. The doping precursor was dispersed by ultrasonication in 1 mL of absolute ethanol and mixed with TIP before addition to hydroalcoholic HDA-KCl.

1-ethyl-3-methylimidazolium bis(trifluoromethanesulfonyl)imide (99%) (EMIMTFSI), lithium bis(trifluoromethanesulfonyl)imide (99%) (LiTFSI) (Solvionic) and LP30 (1 M $LiPF_6$ in ethylene carbonate/dimethyl carbonate 50/50) (95%) (Sigma-Aldrich) were all used as received. The IL-based electrolyte was prepared by mixing 0.5 M LiTFSI in EMIMTFSI and stirring at ambient temperature in the glovebox for 1 hour. Glass fibre separators (Millipore) were dried under vacuum at 100 °C overnight before being transferred into the glovebox for cell assembly.

Working electrodes were prepared by mixing 80 wt% of Nb/TiO_2 powder, 10 wt% Super-P and 10 wt% Kynar in NMP as solvent. The slurry was stirred overnight and then coated onto Cu-foil with a TQC AB3400 motorized automatic film applicator equipped with a stainless-steel doctor blade. The coated film was left to dry at room temperature overnight and then at 80 °C for 12 hours resulting in homogenous 150 μm thick electrodes. The electrodes ($\phi = 10$ mm, 1.8 mg cm^{-2} electrode mass) were transferred into the glove box ($H_2O < 0.1$ ppm, $O_2 < 1$ ppm), dried additionally in a Buchi oven before assembly of 3-electrode cells. Activated carbon (Kuraray YP 50F, 2096 m^2 g^{-1}) was used as counter electrode (10 mm, 4 mg cm^{-2} electrode mass) and was prepared following the same procedure as for the working electrode, but with thickness of 300 μm. The reference electrode was a silver foil (99.99%) (Alfa-Aesar), cleaned with concentrated HCl, rinsed in propanol and dried before use.

Electrochemical measurements were performed using a Biologic VMP-3 potentiostat. Cyclic voltammetry (CV) was performed at 10 mV s^{-1} in the potential window 0 to −2.1 V *vs.* Ag/Ag$^+$. Constant current (CC) cycling was performed with current densities in the range 1–20 A g^{-1} with respect to the electrode mass, starting with the lowest current density. Electrochemical impedance spectroscopy (EIS) was performed in two different frequency intervals, 10 MHz to 10 mHz for the measurements before cycling and 10 MHz to 1 Hz for the in situ measurements in order to reduce the acquisition time. The X-ray diffraction (XRD) measurements were

performed on an X'Pert Pro diffractometer (Cu Kα radiation) equipped with an X'Celerator ultrafast RTMS detector. The cycled samples were washed in dimethyl carbonate and transferred to capillaries for XRD experiments in a glovebox. The capillaries were sealed inside the glovebox to prevent exposure to air. The Rietveld analysis of the obtained XRD patterns was performed using the MAUD software package.[48]

The electrode morphology was investigated by scanning electron microscopy (SEM) on a JSM 7800F instrument.

The XPS measurements were performed using monochromatic Al X-ray source ($E = 1486.6$ eV) with a beam diameter of 100 μm and an energy resolution of 0.646 eV. The samples were washed in dimethyl carbonate and left to dry overnight in the glovebox before being transferred to the XPS sample chamber in a designated transfer chamber ensuring that no exposure to the atmosphere occurred.

Acknowledgements

Eric Tam and Shizhao Xiong are acknowledged for valuable support with the XPS experiments. This research was supported by the Swedish Energy Agency ("Batterifonden" grant #39042-1) and PJ and AMNS are also grateful to the Swedish Energy Agency ("Batterifonden" grant #42762-1) for financial support.

Conflict of Interest

The authors declare no conflict of interest.

Keywords: supercapacitor · TiO_2 · ionic liquid · Nb-doping · improved stability

[1] C. Schütter, S. Pohlmann, A. Balducci, *Adv. Energy Mater.* **2019**, *9*, 1900334.
[2] A. González, E. Goikolea, J. A. Barrena, R. Mysyk, *Renewable Sustainable Energy Rev.* **2016**, *58*, 1189–1206.
[3] P. Acevedo-Peña, M. Haro, M. E. Rincón, J. Bisquert, G. Garcia-Belmonte, *J. Power Sources* **2014**, *268*, 397–403.
[4] P. Kubiak, M. Pfanzelt, J. Geserick, U. Hörmann, N. Hüsing, U. Kaiser, M. Wohlfahrt-Mehrens, *J. Power Sources* **2009**, *194*, 1099–1104.
[5] Q. Wang, Z. Wen, J. Li, *Adv. Funct. Mater.* **2006**, *16*, 2141–2146.
[6] B. Zachau-Christiansen, K. West, T. Jacobsen, S. Atlung, *Solid State Ionics* **1988**, *28–30*, 1176–1182.
[7] J. Y. Shin, D. Samuelis, J. Maier, *Adv. Funct. Mater.* **2011**, *21*, 3464–3472.
[8] L. Kavan, M. Grätzel, J. Rathouský, A. Zukal, *J. Electrochem. Soc.* **1996**, *143*, 394–400.
[9] V. Aravindan, Y.-S. Lee, R. Yazami, S. Madhavi, *Mater. Today* **2015**, *18*, 345–351.
[10] X. Lu, M. Yu, G. Wang, T. Zhai, S. Xie, Y. Ling, Y. Tong, Y. Li, *Adv. Mater.* **2013**, *25*, 267–272.
[11] H. Kim, M. Y. Cho, M. H. Kim, K. Y. Park, H. Gwon, Y. Lee, K. C. Roh, K. Kang, *Adv. Energy Mater.* **2013**, *3*, 1500–1506.
[12] P. C. Chen, S. J. Hsieh, J. Zou, C. C. Chen, *Mater. Lett.* **2014**, *133*, 175–178.
[13] X. Chen, L. Liu, F. Huang, *Chem. Soc. Rev.* **2015**, *44*, 1861–1885.
[14] M. Lübke, I. Johnson, N. M. Makwana, D. Brett, P. Shearing, Z. Liu, J. A. Darr, *J. Power Sources* **2015**, *294*, 94–102.
[15] H. Wu, S. Chang, X. Liu, L. Yu, G. Wang, D. Cao, Y. Zhang, B. Yang, P. She, *Solid State Ionics* **2013**, *232*, 13–18.
[16] P. Kubiak, J. Geserick, N. Hüsing, M. Wohlfahrt-Mehrens, *J. Power Sources* **2008**, *175*, 510–516.
[17] S. W. Oh, S. H. Park, Y. K. Sun, *J. Power Sources* **2006**, *161*, 1314–1318.
[18] N. Zec, N. Cvjetićanin, M. Bešter-Rogač, M. Vraneš, S. Gadžurića, *J. Electrochem. Soc.* **2017**, *164*, H5100–H5107.
[19] K. H. Lee, S. W. Song, *ACS Appl. Mater. Interfaces* **2011**, *3*, 3697–3703.
[20] C. Arbizzani, M. Biso, D. Cericola, M. Lazzari, F. Soavi, M. Mastragostino, *J. Power Sources* **2008**, *185*, 1575–1579.
[21] J. Xiang, F. Wu, R. Chen, L. Li, H. Yu, *J. Power Sources* **2013**, *233*, 115–120.
[22] H. Weber, M. Salanne, B. Kirchner, *J. Phys. Chem. C* **2015**, *119*, 25260–25267.
[23] G. Calcagno, A. Lotsari, A. Dang, S. Lindberg, A. E. C. Palmqvist, A. Matic, C. Cavallo, *Mater. Today Energy* **2020**, *In press*.
[24] M. Fehse, S. Cavaliere, P. E. Lippens, I. Savych, A. Iadecola, L. Monconduit, D. J. Jones, J. Rozière, F. Fischer, C. Tessier, et al., *J. Phys. Chem. C* **2013**, *117*, 13827–13835.
[25] A. J. Gardecka, M. Lübke, C. F. Armer, D. Ning, M. V. Reddy, A. S. Williams, A. Lowe, Z. Liu, I. P. Parkin, J. A. Darr, *Solid State Sci.* **2018**, *83*, 115–121.
[26] A. Latini, C. Cavallo, F. K. Aldibaja, D. Gozzi, D. Carta, A. Corrias, L. Lazzarini, G. Salviati, *J. Phys. Chem. C* **2013**, *117*, 25276–25289.
[27] R. Giannuzzi, M. Manca, L. De Marco, M. R. Belviso, A. Cannavale, T. Sibillano, C. Giannini, P. D. Cozzoli, G. Gigli, *ACS Appl. Mater. Interfaces* **2014**, *6*, 1933–1943.
[28] B. Laskova, M. Zukalova, A. Zukal, M. Bousa, L. Kavan, *J. Power Sources* **2014**, *246*, 103–109.
[29] T. Beuvier, M. Richard-Plouet, L. Brohan, *J. Phys. Chem. C* **2009**, *113*, 13703–13706.
[30] G. Sudant, E. Baudrin, D. Larcher, J. M. Tarascon, *J. Mater. Chem.* **2005**, *15*, 1263–1269.
[31] Y. Wang, M. Wu, W. F. Zhang, *Electrochim. Acta* **2008**, *53*, 7863–7868.
[32] B. Song, S. Liu, J. Jian, M. Lei, X. Wang, H. Li, J. Yu, X. Chen, *J. Power Sources* **2008**, *180*, 869–874.
[33] U. Lafont, D. Carta, G. Mountjoy, A. V. Chadwick, E. M. Kelder, *J. Phys. Chem. C* **2010**, *114*, 1372–1378.
[34] E. Ventosa, E. Madej, G. Zampardi, B. Mei, P. Weide, H. Antoni, F. La Mantia, M. Muhler, W. Schuhmann, *ACS Appl. Mater. Interfaces* **2017**, *9*, 3123–3130.
[35] M. L. Lee, C. Y. Su, Y. H. Lin, S. C. Liao, J. M. Chen, T. P. Perng, J. W. Yeh, H. C. Shih, *J. Power Sources* **2013**, *244*, 410–416.
[36] Y. An, P. Zuo, X. Cheng, L. Liao, G. Yin, *Electrochim. Acta* **2011**, *56*, 4841–4848.
[37] "The Materials Project," can be found under https://materialsproject.org/, entries: mp_758673 and mp_1193296 for Pnnm LiM2O4 (M=Nb and Ti), **n.d**.
[38] A. Jain, S. P. Ong, G. Hautier, W. Chen, W. D. Richards, S. Dacek, S. Cholia, D. Gunter, D. Skinner, G. Ceder, et al., *APL Mater.* **2013**, *1*, DOI 10.1063/1.4812323.
[39] M. Haruta, T. Okubo, Y. Masuo, S. Yoshida, A. Tomita, T. Takenaka, T. Doi, M. Inaba, *Electrochim. Acta* **2017**, *224*, 186–193.
[40] K. Wu, J. Yang, X. Y. Qiu, J. M. Xu, Q. Q. Zhang, J. Jin, Q. C. Zhuang, *Electrochim. Acta* **2013**, *108*, 841–851.
[41] C. Kim, N. S. Norberg, C. T. Alexander, R. Kostecki, J. Cabana, *Adv. Funct. Mater.* **2013**, *23*, 1214–1222.
[42] V. Augustyn, P. Simon, B. Dunn, *Energy Environ. Sci.* **2014**, *7*, 1597.
[43] S. Xiong, K. Xie, E. Blomberg, P. Jacobsson, A. Matic, *J. Power Sources* **2014**, *252*, 150–155.
[44] Y. Preibisch, F. Horsthemke, M. Winter, S. Nowak, A. S. Best, *Chem. Mater.* **2020**, *32*, 2389–2398.
[45] S. Södergren, H. Siegbahn, H. Rensmo, H. Lindström, A. Hagfeldt, S. E. Lindquist, *J. Phys. Chem. B* **1997**, *101*, 3087–3090.
[46] B. K. Kaleji, R. Sarraf-Mamoory, A. Fujishima, *Mater. Chem. Phys.* **2012**, *132*, 210–215.
[47] C. Cavallo, A. Salleo, D. Gozzi, F. Di Pascasio, S. Quaranta, R. Panetta, A. Latini, *Sci. Rep.* **2015**, *5*, 16785.
[48] L. Lutterotti, S. Matthies, H.-R. Wenk, in *Proceeding Twelfth Int. Conf. Textures Mater.*, **1999**, p. 1599.

Manuscript received: April 3, 2020
Revised manuscript received: May 31, 2020
Accepted manuscript online: June 8, 2020
Version of record online: ■■, ■■■

ARTICLES

Subtle effects: A combination of a microbead morphology, Nb-doping, and the use of an ionic liquid electrolyte is shown to significantly decrease the irreversible capacity loss of TiO_2 and improve its electrochemical performance. A change in the electrochemical response in the first cycles indicates formation of a solid-electrolyte interphase (SEI) or a modification of the structure of the surface layer of the TiO_2/Nb microbeads, which apparently stabilises the performance. The change in the response is manifested in an increased charge transfer resistance and the presence of two charge transfer contributions. During prolonged cycling the TiO_2/Nb electrode shows an excellent stability over 5000 cycles.

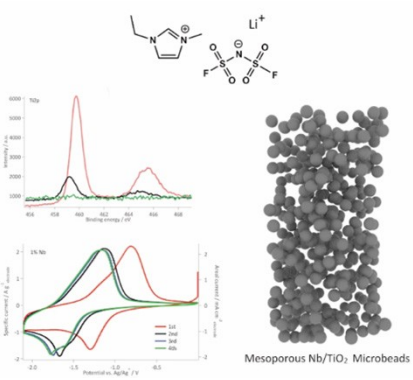

*S. Lindberg, Dr. C. Cavallo, G. Calcagno, Dr. A. M. Navarro-Suárez, Prof. P. Johansson, Prof. A. Matic**

1 – 7

Electrochemical Behaviour of Nb-Doped Anatase TiO_2 Microbeads in an Ionic Liquid Electrolyte